

## Toroics | Hot Paper |

# Oblate versus Prolate Electron Density of Lanthanide Ions: A Design Criterion for Engineering Toroidal Moments? A Case Study on $\{\text{Ln}^{\text{III}}_6\}$ ( $\text{Ln} = \text{Tb}, \text{Dy}, \text{Ho}$ and $\text{Er}$ ) Wheels

Stuart K. Langley<sup>+,\*<sup>[a]</sup></sup> Kuduva R. Vignesh<sup>+,<sup>[b]</sup></sup> Boujema Moubaraki,<sup>[c]</sup> Gopalan Rajaraman,<sup>\*<sup>[d]</sup></sup> and Keith S. Murray<sup>\*<sup>[c]</sup></sup>

**Abstract:** We report four new complexes based on a  $\{\text{Ln}^{\text{III}}_6\}$  wheel structure, three of which possess a net toroidal magnetic moment. The four examples consist of  $\{\text{Tb}^{\text{III}}_6\}$  and  $\{\text{Ho}^{\text{III}}_6\}$  wheels, which are rare examples of non  $\text{Dy}^{\text{III}}$  based complexes possessing a toroidal magnetic ground state, and a  $\{\text{Dy}^{\text{III}}_6\}$  complex which improves its toroidal structure upon

lowering the crystallographic symmetry from trigonal ( $R\bar{3}$ ) to triclinic ( $P\bar{1}$ ). Notably the toroidal moment is lost for the trigonal  $\{\text{Er}^{\text{III}}_6\}$  analogue. This suggests the possibility of utilizing the popular concept of oblate and prolate electron density of the ground state  $M_J$  levels of lanthanide ions to engineer toroidal moments.

## Introduction

The study of the magnetic properties of polynuclear coordination complexes synthesised using lanthanide ions has revealed a plethora of interesting magnetic based phenomena.<sup>[1]</sup> This includes slow relaxation of the magnetization vector which is synonymous with single-molecule magnet (SMM) behaviour,<sup>[2]</sup> a large magnetocaloric effect<sup>[3]</sup> which has applications in magnetic refrigeration<sup>[3]</sup> and a toroidal magnetic structure which is characterized by a vortex distribution of magnetic dipoles.<sup>[4]</sup> Discrete molecules with a toroidal magnetic state have recently been termed as single-molecule toroics (SMTs).<sup>[4a,5]</sup> SMTs are defined as bistable molecules with a toroidal magnetic state,

and seem to be most promising for future applications in quantum computing and information storage. A key feature of toroidal magnetic moments is their insensitivity to homogeneous magnetic fields.<sup>[4a]</sup> This feature can be utilized, since a crucial challenge in the quest for the ultimate miniaturization of spin-devices based on single-molecule magnets involves harnessing molecular spin degrees of freedom that are protected against fast spin relaxation and/or decoherence mechanisms originating from intermolecular coupling thus achieving performing devices without compromising their packing density. Long-range dipole–dipole interactions are clearly an obstacle on the way to such optimal density, as fluctuations of the large SMM magnetic moment can significantly affect the performance of neighbouring devices. One elegant solution against such molecule–molecule disruptive interference consists of harnessing molecular exchange-coupled quantum states characterized by a toroidal magnetic moment and zero magnetic moment, as intermolecular interactions would then decay as quadrupole–quadrupole interactions, that is, they are short range. Moreover, the toroidal magnetic moment interacts with a dc current passing through the molecule or a time-varying electric field by magneto-electric coupling, allowing the moment to be controlled and manipulated purely by electrical means, a property much sought-after for molecular devices.<sup>[6]</sup> For SMTs the vortex arrangement of local magnetic moments is due to a ‘wheel’ metallic topology, or a local wheel-shape arrangement of ions, and specific magnetic interaction between metal sites. Toroidal moments can be influenced by the molecular symmetry and local magnetic moment, as well as magnetic interactions, including dipole and exchange interactions between metal ions.<sup>[4b]</sup> At present, SMTs form a relatively small group of complexes and toroidal moments in molecular systems have predominantly been reported for dysprosium compounds, however, we have recently reported this phenomenon


[a] Dr. S. K. Langley<sup>+</sup>  
School of Science and the Environment, Division of chemistry  
Manchester Metropolitan University  
Manchester (UK)  
E-mail: s.langley@mmu.ac.uk

[b] Dr. K. R. Vignesh<sup>+</sup>  
IITB-Monash Research Academy  
IIT Bombay  
Mumbai, 400076 (India)

[c] Dr. B. Moubaraki, Prof. K. S. Murray  
School of Chemistry  
Monash University  
Clayton, Victoria 3800 (Australia)  
E-mail: keith.murray@monash.edu

[d] Prof. G. Rajaraman  
Department of Chemistry  
Indian Institute of Technology Bombay  
Powai, Mumbai, Maharashtra, 400 076 (India)  
E-mail: rajaraman@chem.iitb.ac.in

[\*] These authors contributed equally to this work.

 Supporting information and the ORCID identification number(s) for the author(s) of this article can be found under:  
<https://doi.org/10.1002/chem.201805765>.

for complexes containing Tb<sup>III</sup> and Ho<sup>III</sup> ions, which offers the possibility of extending this work to other anisotropic lanthanide ions.<sup>[7]</sup>

The advantages of using lanthanide ions, in particular Dy<sup>III</sup>, over transition metals for obtaining SMTs is due to the strong uniaxial magnetic anisotropy of the Dy<sup>III</sup> ions in common low-symmetry ligand environments ( $g_z \gg g_{xy}$ ). Large values of the local magnetic moments on the magnetic sites afford strong intramolecular dipolar coupling, the latter found to be responsible for the toroidal moment of the ground states of complexes investigated. As indicated above, toroidal phenomena have been limited to a small family of Dy<sup>III</sup> complexes, which include triangular {Dy<sup>III</sup><sub>3</sub>}<sup>[4a,5]</sup> planar diamond {Dy<sup>III</sup><sub>4</sub>}<sup>[8]</sup> cubane {Dy<sup>III</sup><sub>4</sub>}<sup>[9]</sup> and wheel {Dy<sup>III</sup><sub>6</sub>} metal topologies.<sup>[10]</sup> Moreover, the combination of two {Dy<sup>III</sup><sub>3</sub>} triangular SMT complexes resulted in a {Dy<sup>III</sup><sub>6</sub>} complex with an enhanced toroidal moment compared to the {Dy<sup>III</sup><sub>3</sub>} building unit.<sup>[11]</sup> One final complex is a coordination polymer connecting {Dy<sup>III</sup><sub>3</sub>} triangles via a Cu<sup>II</sup> ion. This resulted in a zero toroidal magnetic moment where neighbouring {Dy<sup>III</sup><sub>3</sub>} units are opposite in sign and compensate each other owing to the presence of different types of Dy ion in the exchange pathway.<sup>[12]</sup> Recently, we have reported a heptanuclear {Cr<sup>III</sup>Dy<sup>III</sup><sub>6</sub>} complex in which two Dy<sup>III</sup><sub>3</sub> triangles are linked by an octahedral Cr<sup>III</sup> ion. It displays a ferrotoroidal moment brought about by con-rotation of the Dy<sub>3</sub> magnetic quantum states.<sup>[13]</sup>

In previous work, we reported the synthesis of a {Dy<sup>III</sup><sub>6</sub>} wheel (highlighted above)<sup>[10a]</sup> which has a molecular formula of [Dy<sup>III</sup><sub>6</sub>(teaH)<sub>6</sub>(NO<sub>3</sub>)<sub>6</sub>]·8MeOH (**1**) ([teaH]<sup>2-</sup> = doubly deprotonated triethanolamine). The wheel crystallizes in the trigonal, *R* $\bar{3}$  space group, with one unique ion in the asymmetric unit. Powell and co-workers subsequently reported how ligand field variations affected toroidal behaviour in two other related {Dy<sub>6</sub>} wheels.<sup>[14]</sup> In light of the discovery of toroidal moments in {Cr<sup>III</sup>Tb<sup>III</sup><sub>6</sub>} and {Cr<sup>III</sup>Ho<sup>III</sup><sub>6</sub>} complexes<sup>[7]</sup> we have therefore studied whether other anisotropic lanthanide ions are viable candidates to reveal a toroidal magnetic structure in this molecular wheel system, and to determine how the crystallographic symmetry of the molecule affects the toroidal moment. We have, therefore, synthesised; i) analogous hexanuclear wheel complexes containing Tb<sup>III</sup>, Ho<sup>III</sup> and Er<sup>III</sup> ions and ii) crystallized the {Dy<sup>III</sup><sub>6</sub>} wheel in the low symmetry, triclinic, *P* $\bar{1}$  space group. It is expected that the toroidal moment will be sensitive to the metal ion used due to the transition from a prolate to oblate distribution of electron density in the ground magnetic microstate, which will dictate the direction of the single ion anisotropy axis.<sup>[7]</sup> The crystallographic symmetry should also play a role in directing the anisotropy axes of the single ions. To determine how the toroidal magnetic moment is modified upon changing the lanthanide ion and on the crystallographic symmetry we have studied this phenomenon from both an experimental and a theoretical perspective.

Herein, we report the synthesis and structural characterization of four new complexes of molecular formula [Ln<sup>III</sup><sub>6</sub>(teaH)<sub>6</sub>(NO<sub>3</sub>)<sub>6</sub>]·8MeOH (Ln = Tb (**2**), Ho (**3**) and Er (**4**)) and [Dy<sup>III</sup><sub>6</sub>(teaH)<sub>6</sub>(NO<sub>3</sub>)<sub>6</sub>]·3DMF·H<sub>2</sub>O (**5**) and detail their magnetic behaviour and provide an ab initio analysis. We reveal how the

toroidal moment is maintained for the {Tb<sup>III</sup><sub>6</sub>} and {Ho<sup>III</sup><sub>6</sub>} complexes, but is lost for the {Er<sup>III</sup><sub>6</sub>} wheel and that the toroidal moment is maintained upon lowering the crystallographic symmetry in the {Dy<sup>III</sup><sub>6</sub>} complex.

## Experimental Section

### General information

The reactions were carried out under aerobic conditions. Chemicals and solvents were obtained from commercial sources and used without further purification.

**Synthesis of [Tb<sup>III</sup><sub>6</sub>(teaH)<sub>6</sub>(NO<sub>3</sub>)<sub>6</sub>]·8MeOH (**2**):** Tb(NO<sub>3</sub>)<sub>3</sub>·6H<sub>2</sub>O (0.22 g, 0.5 mmol) was dissolved in MeOH/CH<sub>2</sub>Cl<sub>2</sub> (5 mL:15 mL), followed by the addition of triethanolamine (0.07 mL, 1 mmol) and triethylamine (0.55 mL, 4.0 mmol). This resulted in a colourless solution, which was stirred for 4 hours. After this time a small amount of precipitate had formed. The solution was filtered and layered with diethyl ether (Et<sub>2</sub>O). Within 1–2 days colourless crystals of **2** had appeared, in approximate yield of 53% (crystalline product). Calculated (found) for **2**: Tb<sub>6</sub>C<sub>44</sub>H<sub>110</sub>O<sub>44</sub>N<sub>12</sub>: C, 21.44 (21.55); H, 4.50 (4.81); N, 6.82(6.92).

**Synthesis of [Ho<sup>III</sup><sub>6</sub>(teaH)<sub>6</sub>(NO<sub>3</sub>)<sub>6</sub>]·8MeOH (**3**):** The same procedure used for **2** was followed, but Ho(NO<sub>3</sub>)<sub>3</sub>·6H<sub>2</sub>O was used in place of Tb(NO<sub>3</sub>)<sub>3</sub>·6H<sub>2</sub>O. This resulted in a colourless solution, which was stirred for 4 hours. After this time a small amount of precipitate had formed. The solution was filtered and layered with diethyl ether (Et<sub>2</sub>O). Within 1–2 days' colourless crystals of **3** had appeared, in approximate yield of 65% (crystalline product). Calculated (found) for **3**: Ho<sub>6</sub>C<sub>44</sub>H<sub>110</sub>O<sub>44</sub>N<sub>12</sub>: C, 21.13 (21.41); H, 4.43 (4.37); N, 6.72 (6.74).

**Synthesis of [Er<sup>III</sup><sub>6</sub>(teaH)<sub>6</sub>(NO<sub>3</sub>)<sub>6</sub>]·8MeOH (**4**):** The same procedure used for **2** was followed, but Er(NO<sub>3</sub>)<sub>3</sub>·6H<sub>2</sub>O was used in place of Tb(NO<sub>3</sub>)<sub>3</sub>·6H<sub>2</sub>O. This resulted in a colourless solution, which was stirred for 4 hours. After this time a small amount of precipitate had formed. The solution was filtered and layered with diethyl ether (Et<sub>2</sub>O). Within 1–2 days' colourless crystals of **4** had appeared, in approximate yield of 61% (crystalline product). Calculated (found) for **4**: Er<sub>6</sub>C<sub>44</sub>H<sub>110</sub>O<sub>44</sub>N<sub>12</sub>: C, 21.01 (21.15); H, 4.41 (4.47); N, 6.68 (6.83).

**Synthesis of [Dy<sup>III</sup><sub>6</sub>(teaH)<sub>6</sub>(NO<sub>3</sub>)<sub>6</sub>]·3DMF·H<sub>2</sub>O (**5**):** The same procedure used for **2** was followed, but Dy(NO<sub>3</sub>)<sub>3</sub>·6H<sub>2</sub>O was used in place of Tb(NO<sub>3</sub>)<sub>3</sub>·6H<sub>2</sub>O and dimethylformamide (DMF) was used as solvent. This resulted in a colourless solution, which was stirred for 4 hours. The solution was layered with diethyl ether (Et<sub>2</sub>O) and within 1–2 days, colourless crystals of **5** had appeared, which could be isolated in approximate yield of 43% (crystalline product). Calculated (found) for **5**: Dy<sub>6</sub>C<sub>45</sub>H<sub>101</sub>O<sub>40</sub>N<sub>15</sub>: C, 21.91 (21.54); H, 4.13 (4.27); N, 8.52 (8.12).

**X-ray crystallography:** X-ray measurements for **2–4** were performed at 123(2) K using a Bruker Smart Apex X8 diffractometer with MoK $\alpha$  radiation. The data collection and integration were performed within SMART and SAINT + software programs, and corrected for absorption using the Bruker SADABS program. Measurements for compound **5** were performed at 123(2) K at the Australian synchrotron MX1 beam-line. The data collection and integration were performed within Blu-Ice<sup>[15]</sup> and XDS<sup>[16]</sup> software programs. Compounds **2–5** were solved by direct methods (SHELXS-97)<sup>[17]</sup> and refined (SHELXL-97)<sup>[18]</sup> by full least matrix least-squares on all *F*<sup>2</sup> data.<sup>[19]</sup> Crystallographic data and refinement parameters are summarized in Table S1. Crystallographic details are available in the Supporting Information (SI) in CIF format. CCDC 1876161 (**2**),

1876164 (3), 1876163 (4), and 1876162 (5) contain the supplementary crystallographic data for this paper. These data can be obtained free of charge from The Cambridge Crystallographic Data Centre.

**Magnetic measurements:** The magnetic susceptibility measurements were carried out on a Quantum Design SQUID magnetometer MPMS-XL 7 operating between 1.8 and 300 K for dc-applied fields ranging from 0–5 T. Microcrystalline samples were dispersed in Vaseline in order to avoid torquing of the crystallites. The sample mulls were contained in a calibrated gelatine capsule held at the centre of a drinking straw that was fixed at the end of the sample rod. Alternating current (ac) susceptibility measurements were carried out under an oscillating ac field of 3.5 Oe and frequencies ranging from 0.1 to 1500 Hz using both zero and 2000 Oe static dc fields.

### Computational details

Using MOLCAS 8.0,<sup>[20]</sup> ab initio calculations were performed on the Ln<sup>III</sup> ions using their crystal structures. Relativistic effects are taken into account on the basis of the Douglas-Kroll Hamiltonian.<sup>[21]</sup> The spin-free Eigen states are achieved by the Complete Active Space Self-Consistent Field (CASSCF) method.<sup>[22]</sup> We have employed the [ANO-RCC.<sup>[23]</sup> 8s7p5d3f2g1h.] basis set for Ln<sup>III</sup> atoms, the [ANO-RCC.3s2p.] basis set for C atoms, the [ANO-RCC.2s.] basis set for H atoms, the [ANO-RCC.3s2p1d.] basis set for N atoms, the [ANO-RCC.7s6p4d2f.] basis set for the Lu atom, and the [ANO-RCC.3s2p1d.] basis set for O atoms. Here, we included eight electrons across seven 4f orbitals of the Tb<sup>3+</sup> ion, nine electrons across seven 4f orbitals of the Dy<sup>3+</sup> ion, ten electrons across seven 4f orbitals of the Ho<sup>3+</sup> ion and eleven electrons across seven 4f orbitals of the Er<sup>3+</sup> ion. Then using these guess orbitals, we have chosen the active space based on the number of active electrons in the number of active orbitals and carried out the SA-CASSCF calculations. Here, 21 roots in the Configuration Interaction (CI) procedure were computed for Dy<sup>3+</sup> ion. Similarly, we considered seven septet excited states, one hundred and forty quintet excited states and one hundred and ninety-five triplet excited states for Tb<sup>3+</sup> ion, and thirty-five quintet excited states, two hundred and ten triplet excited states and one hundred and ninety-five singlet excited states for Ho<sup>3+</sup> ion and thirty-five quartet excited states, one hundred and twelve doublet excited states for Er<sup>3+</sup> ion in the calculations to compute the anisotropy. All the excited states corresponding to each multiplets of ions have been computed in the CASSCF module. After computing these excited states, we have mixed all the low-lying excited states (< 50 000 cm<sup>-1</sup>) using the RASSI-SO<sup>[24]</sup> module to calculate the spin-orbit coupled states. Moreover, these computed SO states have been considered into the SINGLE\_ANISO<sup>[25]</sup> program to compute the *g*-tensors. Crystal-field parameters have been extracted using the SINGLE\_ANISO code, as implemented in MOLCAS 8.0. We have used the Loprop charges estimated using ab initio calculations to understand the direction of magnetic anisotropy which is a static property, that can be computed like a charge, a component of the dipole moment or an exchange-hole dipole moment,<sup>[26]</sup> is localized by transforming the property of two centres.<sup>[27]</sup>

The exchange/dipolar interactions between neighbouring Ln<sup>III</sup>–Ln<sup>III</sup> ions have been computed by fitting with the experimental data using POLY\_ANISO module incorporated in MOLCAS suite.<sup>[28]</sup> The exchange Hamiltonian adapted for complexes 2–5 are shown below.

$$\hat{H}_{\text{ex}} = - \sum_{i=1}^3 J_i \cdot S_i \cdot S_{i+1} \quad (1)$$

(here  $J_i = J_i^{\text{dip}} + J_i^{\text{exch}}$ ; that is,  $J_i$  are the total magnetic interaction of the calculated  $J_i^{\text{dip}}$  and fitted  $J_i^{\text{exch}}$  parameters; this describes the interaction between all the neighbouring metal centres).

## Results and Discussion

### Structural analysis

Single crystal X-ray analysis reveal that compounds 2–4 crystallize in the trigonal space group,  $R\bar{3}$ , with the asymmetric unit containing one Ln<sup>III</sup> ion. Compound 5 crystallizes in the triclinic space group,  $P\bar{1}$ , with the asymmetric unit containing two half wheels, each consisting of three Ln<sup>III</sup> ions, with the complete wheel in both cases being generated by inversion symmetry. The metal topology and first coordination sphere are identical for 2–5. As expected it is found that these are hexanuclear species containing six Ln<sup>III</sup> ions, with a planar wheel metallic core structure (Figure 1). The wheel is stabilized by six [teaH]<sup>2-</sup> and six nitrate ligands. Each of the six [teaH]<sup>2-</sup> ligands coordinate to a Ln<sup>III</sup> site via the N-atom. The two deprotonated O-atoms then chelate and bridge from the Ln<sup>III</sup> site to two adjacent Ln<sup>III</sup> ions. Each ligand therefore bridges to three ions in total. The

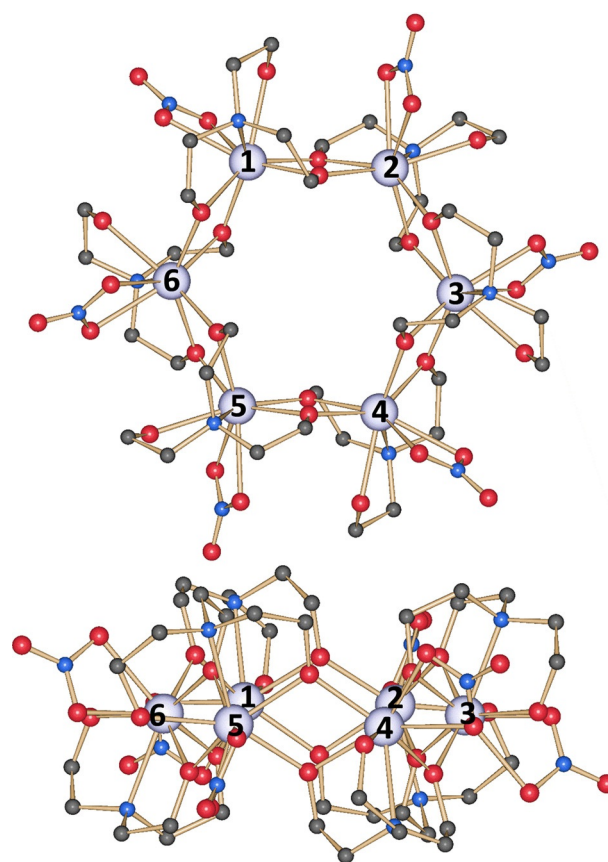


**Figure 1.** The molecular structure of complex 2. The solvent and H atoms are omitted for clarity. Colour Scheme: Tb<sup>III</sup>, violet; O, red; N, blue; C, light grey. Compounds 3–5 have the same metal topology as 2.

third protonated alcohol arm chelates to the Ln<sup>III</sup> site that is bonded to the N-atom. Each of the six (NO<sub>3</sub>)<sup>-</sup> ions chelate to a single Ln<sup>III</sup> ion, completing the coordination sphere of the ion. The Ln<sup>III</sup> ions are eight coordinate in **2–5**, with triangular dodecahedron geometries with the deviations of 2.2, 2.1, 2.0 and 2.4 as predicted by SHAPE software.<sup>[29]</sup>

The average Ln–O bond length is found to be 2.38 Å (Tb, **2**), 2.36 Å (Ho, **3**), 2.36 Å (Er, **4**) and 2.37 Å (Dy, **5**) [cf. 2.36 Å (Dy, **1**)]. Selected bond lengths and angles for **1–4** and **5** are shown in Tables 1 and 2, respectively. Due to the crystallo-

**Table 1.** Selected structural parameters for **1–4** (trigonal, *R*3̄).

	1-Dy <sub>6</sub>	2-Tb <sub>6</sub>	3-Ho <sub>6</sub>	4-Er <sub>6</sub>
Ln...Ln (intramolecular) [Å]	3.730	3.750	3.715	3.707
Ln–O–Ln' [°]	108.36	109.00	108.37	108.38
Ln–O'–Ln' [°]	111.79	112.30	112.22	112.63
Ln...Ln (closest intermolecular) [Å]	8.935	8.957	8.908	8.940

**Table 2.** Selected structural parameters for **5** (triclinic, *P*1̄). Two unique half molecules are found in the asymmetric unit (three unique Dy<sup>III</sup> ions per half).

Molecule 1		Molecule 2	
Dy...Dy	3.742 Å	Dy...Dy	3.743 Å
Dy...Dy	3.714 Å	Dy...Dy	3.716 Å
Dy...Dy'	3.738 Å	Dy...Dy'	3.720 Å
Dy–O–Dy	109.33°	Dy–O–Dy	109.39°
Dy–O–Dy	111.17°	Dy–O–Dy	111.51°
Dy–O–Dy	109.14°	Dy–O–Dy	109.08°
Dy–O–Dy	111.48°	Dy–O–Dy	110.46°
Dy–O–Dy	108.81°	Dy–O–Dy	108.80°
Dy–O–Dy	110.09°	Dy–O–Dy	110.80°
Ln...Ln (closest intermolecular)	7.999 Å		

graphic symmetry, complexes **1–4** pack in the crystal in an identical manner (Figure S1, top). Comparing the closest intramolecular Ln...Ln distance for **1–4** reveals a decrease as we move across the f-block (Tb→Er) as expected. The closest intermolecular Ln...Ln distance also decreases between molecules as we move across the f-block up to {Ho<sub>6</sub>}, where it is then found to increase between {Er<sub>6</sub>} molecules. No notable trend is found for the bond angles; however, it is noted that the smallest Ln–O–Ln angles are found for **1-Dy**.

Comparing **1–4** (trigonal) to **5** (triclinic) we find that the major difference is the packing of the molecules in the crystal (Figure S1), with a much shorter nearest neighbour Ln...Ln intermolecular distance found for **5** (≈8.9 Å (**1–4**) versus ≈8.0 Å (**5**)).

### Magnetic properties

DC magnetic susceptibility data were collected for **2–5** and the variation of  $\chi_M T$  with temperature is shown in Figure 2. The room temperature  $\chi_M T$  product of 70.97, 84.39, 68.82 and 84.56 cm<sup>3</sup>K mol<sup>-1</sup> for **2–5**, respectively, is in agreement with the values expected (70.92, 84.42, 68.88 and 85.02 cm<sup>3</sup>K mol<sup>-1</sup>)

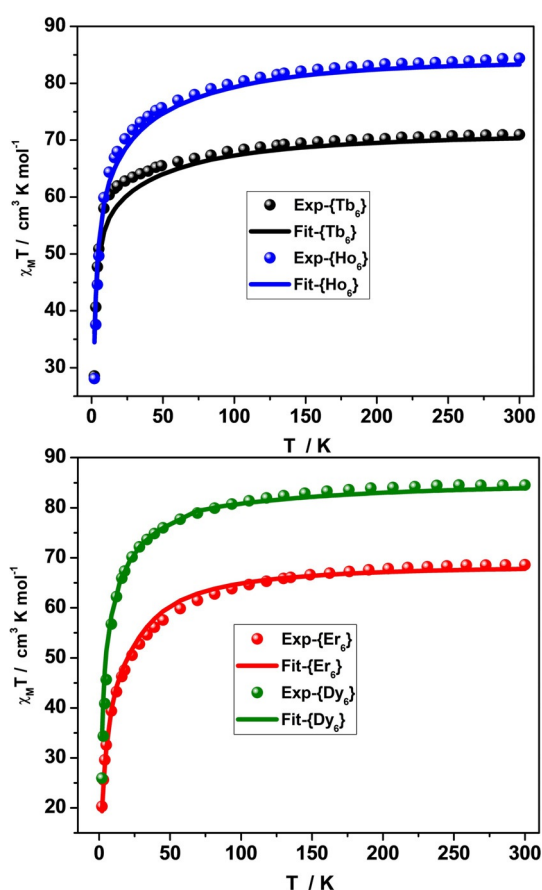


**Figure 2.**  $\chi_M T$  versus  $T$  plots for **2–5** at an applied dc magnetic field of 1 T. The solid lines are POLY ANISO<sup>[28]</sup> fits of the data (see text in the theoretical section).

for six Tb<sup>III</sup> ( $S=3$ ,  $L=3$ ,  ${}^7F_6$ ,  $g=3/2$ ,  $C=11.82$  cm<sup>3</sup>K mol<sup>-1</sup>), six Ho<sup>III</sup> ( $S=2$ ,  $L=6$ ,  ${}^5I_8$ ,  $g=5/4$ ,  $C=14.07$  cm<sup>3</sup>K mol<sup>-1</sup>), six Er<sup>III</sup> ( $S=3/2$ ,  $L=6$ ,  ${}^4I_{15/2}$ ,  $g=6/5$ ,  $C=11.48$  cm<sup>3</sup>K mol<sup>-1</sup>) and six Dy<sup>III</sup> ( $S=5/2$ ,  $L=15/2$ ,  ${}^6H_{15/2}$ ,  $g=4/3$ ,  $C=14.17$  cm<sup>3</sup>K mol<sup>-1</sup>) ions that are non-interacting. As the temperature is reduced the  $\chi_M T$  product (at  $H=1$  T) decreases gradually between room temperature and 50 K, before a more rapid decrease occurs below this temperature. The decrease in  $\chi_M T$  at higher temperatures is attributed to the depopulation of the excited  $m_j$  micro states of the Tb<sup>III</sup>, Ho<sup>III</sup>, Er<sup>III</sup> and Dy<sup>III</sup> ions, the profile also suggests the possibility of antiferromagnetic magnetic exchange interactions (see analysis later). The isothermal  $M$  versus  $H$  plots (Figure 3) at low fields revealed a non-linear, S-shaped curve for **3**, which suggests the presence of a toroidal moment<sup>[4a,5]</sup> and/or possible blockage of the magnetization vector. For **2**, **4** and **5** this is not observed, however this does not preclude SMT behaviour.

To probe for SMM behaviour, the magnetization dynamics were investigated by alternating current (ac) susceptibility measurements as a function of both temperature and frequency. A 3.5 Oe ac field was employed, utilizing both a zero static and a 2000 Oe dc field. Complexes **2** and **3** display a broad weak non-zero out-of-phase susceptibility ( $\chi_M''$ ) signal in a zero-dc field. No out-of-phase signal is found for **4**, however a clear increase in  $\chi_M''$  is observed for **5** at the lowest temperatures probed (Figure S2). The broad out-of-phase signal found

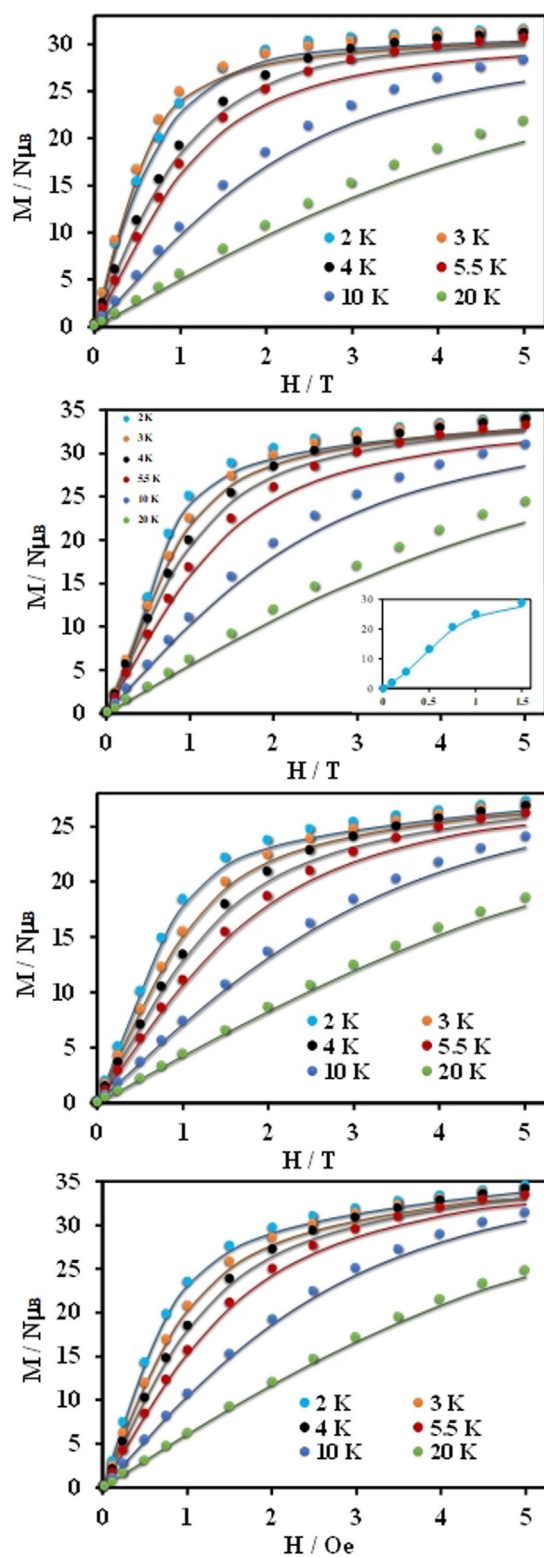


**Figure 3.** The measured and the fitted (POLY ANISO)<sup>[26]</sup> molar magnetization for (top) 2; (middle 1) 3, inset, magnetization at lower field to show S-shape at 2 K; (middle 2) 4 and (bottom) 5.

for 2 and 3, was also observed for 1 from previous work.<sup>[10a]</sup> For most lanthanide SMMs the probability of observing QTM is very high especially for non-Kramer's ions such as Tb<sup>III</sup> and Ho<sup>III</sup>. We have therefore probed the relaxation dynamics under

the application of a static dc magnetic field. All four complexes display an increase in the  $\chi_M''$  signal below  $\sim 10$  K (Figure S3). For 2 and 4 frequency dependent maxima are found, however for 3 and 5 the data are very noisy, and no reliable maxima can be determined. For 2 and 4 fitting the data to the Arrhenius law ( $\tau = \tau_0 \exp(U_{\text{eff}}/k_B T)$ ) a thermally activated barrier  $U_{\text{eff}}$  is estimated to be 23 K and 39 K for 2 and 4, respectively (Figure S4). These results do not unequivocally prove SMM behaviour, but suggests the possibility of such, with a small energy barrier to magnetic reorientation and fast relaxation times, especially via QTM. Because of the fast-magnetic relaxation times, even at temperatures below 2 K, it is suggested that the low field magnetization behaviour points to the presence of a toroidal magnetic moment.

### Theoretical analysis

To probe the nature of the magnetic anisotropy and the mechanism of magnetic relaxation and, more importantly, the possible toroidal nature of the anisotropy axes in these systems, ab initio calculations were undertaken using established procedures employing the MOLCAS 8.0 suite.<sup>[20]</sup> Initially we will focus on single ion Ln<sup>III</sup> calculations and discuss their magnetization characteristics and later expand this to the complete exchange-coupled systems, analysing the nature of exchange and the toroidal behaviour.

### Mechanism of relaxation based on single-ion Ln<sup>III</sup> calculations

Using MOLCAS 8.0 with the CASSCF/RASSI/SINGLE ANISO routine, ab initio calculations were performed on the mononuclear Ln fragments of each {Ln<sup>III</sup><sub>6</sub>} (Ln = Tb (2), Ho (3), Er (4) and Dy (5)) wheel complex (See Figure 1), using the structural data from the single crystal X-ray experiments. Considering all the Ln<sup>III</sup> ions have the same ligand environment, we performed calculations on one Ln<sup>III</sup> ion in the wheel to ensure the intricate details of the structure are captured in the calculations. Since the complete molecule is too large to perform these types of calculations, we have fragmented the wheel into a trinuclear species and have substituted neighbouring ions with a diamagnetic Lu<sup>III</sup> ion. The model fragment is shown in Figure S5. The computed  $g$ -tensors and the energy values of the Ln<sup>III</sup> ions in all four complexes are tabulated in Tables 3 and S2–S4 in the Supporting Information.

The local  $g$ -tensors of each Ln<sup>III</sup> ion in the ground Ising doublet of 2 (Tb<sup>III</sup>) and 3 (Ho<sup>III</sup>) and ground Kramer's doublet (KD) of 5 (Dy<sup>III</sup>) are Ising in nature with a large  $g_z$  parameter (Table 3). Although the local  $g$ -tensors of each Er<sup>III</sup> ion in the ground KD of 4 are axial, they contain a relatively large transverse component ( $g_x$ , and  $g_y$ ) indicating the likelihood of fast QTM in zero static field, thus no slow relaxation of the magnetization is expected. The largest Lprop<sup>[26]</sup> charges are observed for the bridging amine alcohol O-atoms in all four complexes, with smaller charges found on the nitrate O-atoms. Thus, the anisotropy axes align towards the amine alcohol O-atoms for the oblate ions (Tb<sup>III</sup>, Dy<sup>III</sup>, Ho<sup>III</sup>) and align towards the nitrate O-atoms for the prolate Er<sup>III</sup> ion. The orientations of the main

**Table 3.** Low-lying energies ( $\text{cm}^{-1}$ ) and  $g$ -tensors of Ln fragments that originate from the corresponding ground atomic multiplets.

	Tb	Ho	Er	Dy
	0.0	0.0	0.0	0.0
	0.1	3.2	68.4	160.9
	186.9	53.0	107.6	264.5
	189.1	64.1	137.5	360.5
	326.9	83.4	190.6	387.3
	340.9	103.0	229.3	479.8
	432.6	133.7	281.6	632.5
	479.4	150.0	456.7	710.2
	508.2	165.8		
	554.3	192.0		
	555.1	225.7		
	603.4	250.1		
	606.0	274.4		
	Ground Ising Doublets		Ground Kramers doublets	
$g_x$	0.0000	0.0000	0.1163	0.0119
$g_y$	0.0000	0.0000	0.9117	0.0211
$g_z$	17.7233	17.5285	16.3606	19.9095

anisotropy axes in the ground Ising doublets of **2** and **3** and the ground KDs of **4** and **5** are shown in Figures 4 and S6.

The computed energy gap between the ground Ising doublets (for **2** and **3**) or the ground KDs (for **4** and **5**) and the excited states are shown in Tables 3 and S2 of the ESI. For the non-Kramer's ions ( $\text{Tb}^{\text{III}}$  and  $\text{Ho}^{\text{III}}$ ) the energy gap between the ground and the first excited Ising doublets are found to be  $186.9 \text{ cm}^{-1}$  for  $\text{Tb}^{\text{III}}$  ion in **2** and  $53.0 \text{ cm}^{-1}$  for  $\text{Ho}^{\text{III}}$  ion in **3**. We note however,  $\text{Ho}^{\text{III}}$  ion has a large ground state tunnel splitting ( $3.2 \text{ cm}^{-1}$ ) compared to **2** ( $0.1 \text{ cm}^{-1}$ ) (Table 3). Consequently, magnetic relaxation is expected to occur between the ground state doublets on all  $\text{Ln}^{\text{III}}$  ions in zero applied magnetic field. Interestingly, however, we find weak out-of-phase signals from the experimental data. This suggests the exchange interaction could possible quench the QTM leading to blocking of the magnetization at low temperatures. For complexes **4** and **5** containing Kramer's ions ( $\text{Er}^{\text{III}}$  and  $\text{Dy}^{\text{III}}$ ), the energy gap between the ground and the first excited KD is calculated to be  $68.4 \text{ cm}^{-1}$  for  $\text{Er}^{\text{III}}$  ions and  $160.9 \text{ cm}^{-1}$  for  $\text{Dy}^{\text{III}}$  ions, respectively. A qualitative mechanism for the single ion magnetic relaxation for the  $\text{Er}^{\text{III}}$  ion and  $\text{Dy}^{\text{III}}$  ion obtained from the single ion calculations is shown in Figure 5. It is found that the ground-state tunnelling probability is relatively large for both  $\text{Ln}^{\text{III}}$  ions in **4** and **5**, and therefore relaxation of magnetization is expected to occur via ground-state QTM. It is also calculated that the thermally assisted QTM involving the first excited states and an Orbach/Raman mechanism are operational. For **4**, due to the larger tunnelling probability in the ground state KD, compared to **5**, it is predicted that the ground state QTM relaxation process dominates and no SMM behaviour is likely in zero magnetic field. This is backed up by experiments. On the other hand, an out-of-phase signal is found for **5** in zero magnetic field reflecting the lower ground state tunnel probability. In all cases, calculations suggest that the application of a static dc field is expected to quench the QTM between the ground states and leading to longer relaxation times, in line with the experimental measurements.

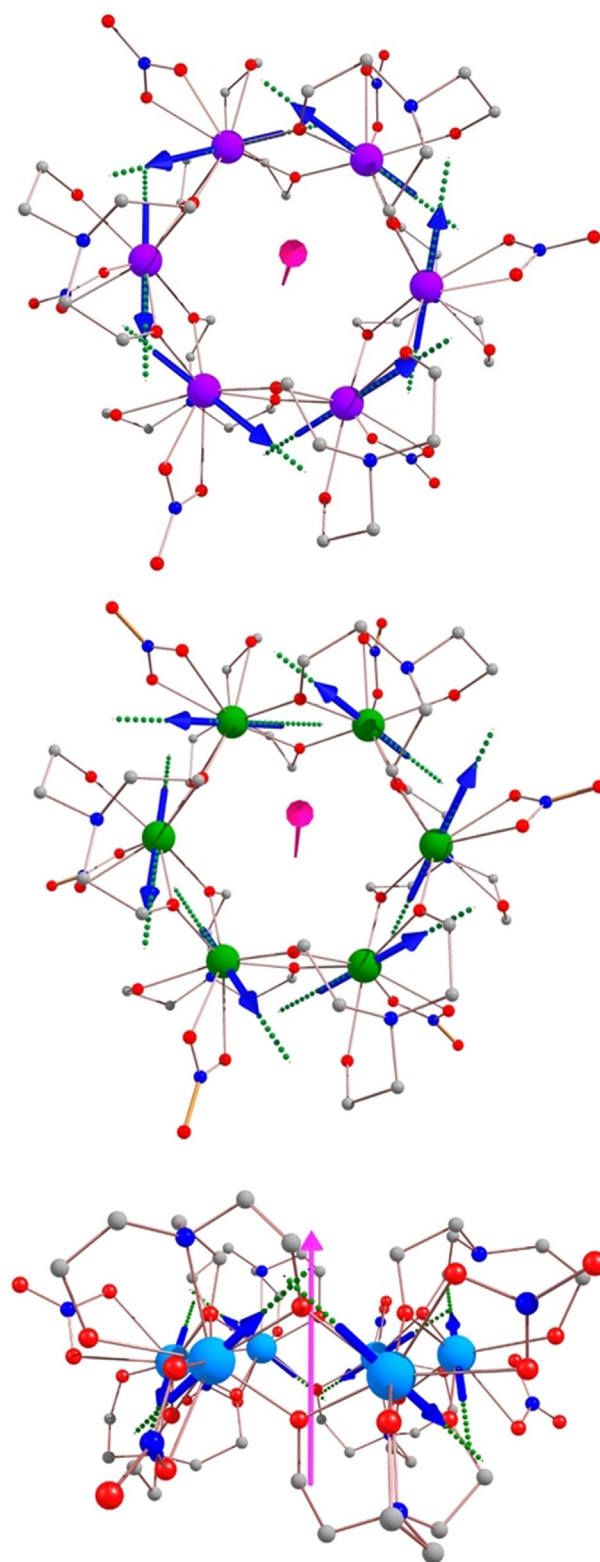


**Figure 4.** The directions of the local anisotropy axes in the ground doublets on the Ln sites (green dashed lines) and of the local magnetic moments (blue arrows) in the ground exchange doublet of (top) **2** { $\text{Tb}_6$ }; (middle) **3** { $\text{Ho}_6$ }; and (bottom) **5** { $\text{Dy}_6$ } (side view). The  $S_6$  axis is shown as a pink arrow.

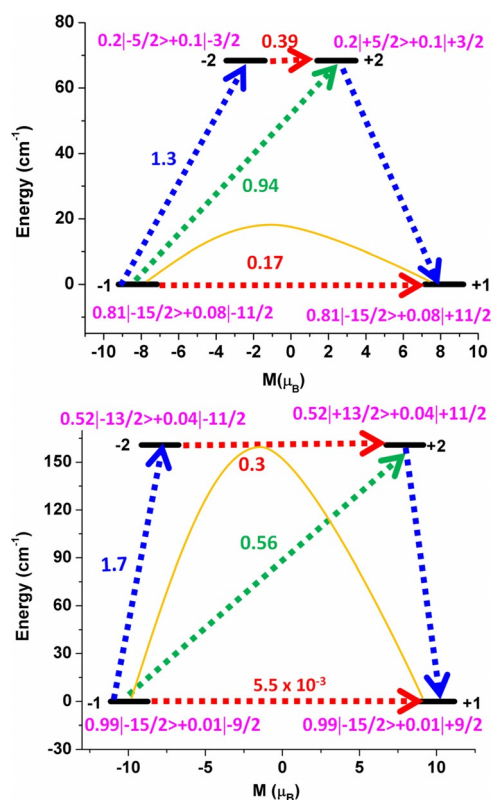


**Figure 5.** The ab initio computed magnetization blocking barrier for (top) the Er<sup>III</sup> ion in **4**; and (bottom) the Dy<sup>III</sup> ion in **5**. The thick black line indicates the Kramer's doublets as a function of computed magnetic moment. The green/blue arrows show the possible pathway through Orbach/Raman relaxation. The dotted red lines represent the presence of QTM/TA-QTM between the connecting pairs. The numbers provided at each arrow are the mean absolute value for the corresponding matrix element of transition magnetic moment. The yellow curve indicates the possible relaxation pathway.

### Probing toroidal behaviour and mechanism of relaxation on exchange-coupled systems

Using the POLY ANISO program<sup>[28]</sup> the exchange and dipolar interactions between nearest-neighbour Ln<sup>III</sup> sites of **2–5** were simulated using Lines model and these values are tabulated in Table 4. The dipolar interaction is included when computing the magnetic exchange parameters ( $J_{tot}$ ). By employing the exchange constants ( $J_{exch} + J_{dip}$ ), good fits to both the susceptibility and the magnetization data were achieved for all complexes (Figure 2 and 3). We found that by including the magnetic dipolar coupling term, we obtain a large coupling constant for all complexes (antiferromagnetic) and the interaction is mainly

**Table 4.** POLY\_ANISO<sup>[28]</sup> fitted exchange and dipolar couplings (cm<sup>-1</sup>) between Ln<sup>III</sup>-Ln<sup>III</sup> of **2–5**. Here  $zJ$  is the intermolecular interaction. The values of 1 taken from ref. 10b for comparison.

Complex	$J_{exch}$	$J_{dip}$	$J_{tot}$	$zJ$
<b>1</b>	0.05	-4.16	-4.11	-
<b>2</b>	-0.17	-3.4	-3.57	-0.02
<b>3</b>	-0.60	-4.30	-4.90	-0.02
<b>4</b>	-0.82	-0.3	-1.12	-0.01
<b>5</b>	-0.05	-9.2	-9.25	-0.01

due to the magnetic dipolar coupling interaction rather than super-exchange pathways. Such strong dipolar coupling interactions between lanthanide ions have been noted for several Dy<sup>III</sup>-based magnets<sup>[10b,30]</sup> which have been crucial in the stabilization and observation of toroidal magnetic states.<sup>[13]</sup>

To understand the nature of the dipolar coupling interaction between two Ln<sup>III</sup> ions, equation (2)<sup>[31]</sup> can be used:

$$E_{dip} = -\left\{\frac{\mu_0}{4\pi}\right\} \frac{\mu_i \mu_j}{r^3} [3 \cos^2(\theta) - 1] \quad (2)$$

in which  $\theta$  is the angle between the orientation of the magnetic moments and the vector connecting two interacting centres. This equation suggests antiferromagnetic coupling for  $\theta > 54.75^\circ$  and ferromagnetic coupling for  $\theta < 54.75^\circ$ . As reported earlier,<sup>[31b]</sup> a larger tilt angle results in antiferromagnetic coupling, leading to antiferromagnetic interactions between the neighbouring Ln<sup>III</sup> ions. In the present case, the angle ( $\theta$ ) between the orientation of magnetic anisotropy and the vector connecting two Ln centres is found to be larger than  $54.75^\circ$  ( $78.2^\circ$ ,  $81.0^\circ$ ,  $62.9^\circ$  and  $87.4^\circ$  for **2**, **3**, **4** and **5**, respectively) and that causes an antiferromagnetic dipolar contribution to the net magnetic exchange for all complexes. The size of the angle ( $\theta$ ) reflects the strength of the antiferromagnetic dipolar coupling, the larger the angle the stronger the exchange parameter. We note that the largest  $J_{exch}$  value is witnessed between the Er<sup>III</sup> ions and such values have been reported earlier in other systems.<sup>[32]</sup>

In **2–5**, the tunnelling gap of the ground exchange coupled states is small (see Table S5–S8 and Figure 6) and will not cause magnetic relaxation in the ground state. Furthermore, Table S5–S8 (in the Supporting Information) show that the coupled excited states are very close in energy resulting in fast relaxation of magnetization at 0.83, 0.25, 3.19 and 4.79 cm<sup>-1</sup> for **2**, **3**, **4** and **5**, respectively (see Figure 6). This supports the experimental observation of lack of a maximum in the experimental out-of-phase ac magnetic susceptibility in zero static field. The magnetization is found to relax via these energy states leading to lower barrier heights.

The direction of the local anisotropy axes on all Ln<sup>III</sup> sites are shown in Figure 4 by dashed lines. The angle of these axes with the main symmetry axis of the complex ( $S_6$ ) is  $83^\circ$  in **2**,  $84^\circ$  in **3**,  $20^\circ$  in **4** and  $77^\circ$  in **5**. The direction of the spins along the main anisotropy axes on each Ln<sup>III</sup> ion for **2**, **3** and **5** are following each other, thus forming a circular pattern resulting in a toroidal magnetic moment and single molecule toric (SMT) behaviour. The toroidal state is not witnessed for **4**. The dipolar interaction between two Ln<sup>III</sup> ions (computed using Eq. 2) plays the main role in deciding the spin-projection of the magnetic anisotropy direction in each exchange coupled state, either clockwise or anticlockwise and it stabilises the toroidal ground state for **2**, **3**, and **5**.<sup>[7,13]</sup> The presence of large antiferromagnetic dipolar coupling and the  $S_6$  symmetry of the complexes causes local magnetic moments on Ln<sup>III</sup> centres in **2**, **3** and **5** to compensate each other in the ground exchange state, leading to negligible or no magnetic moment ( $0.36 \mu_B$  for **2**,  $0.54 \mu_B$  for **3** and  $0.005 \mu_B$  for **5**), similar to that reported

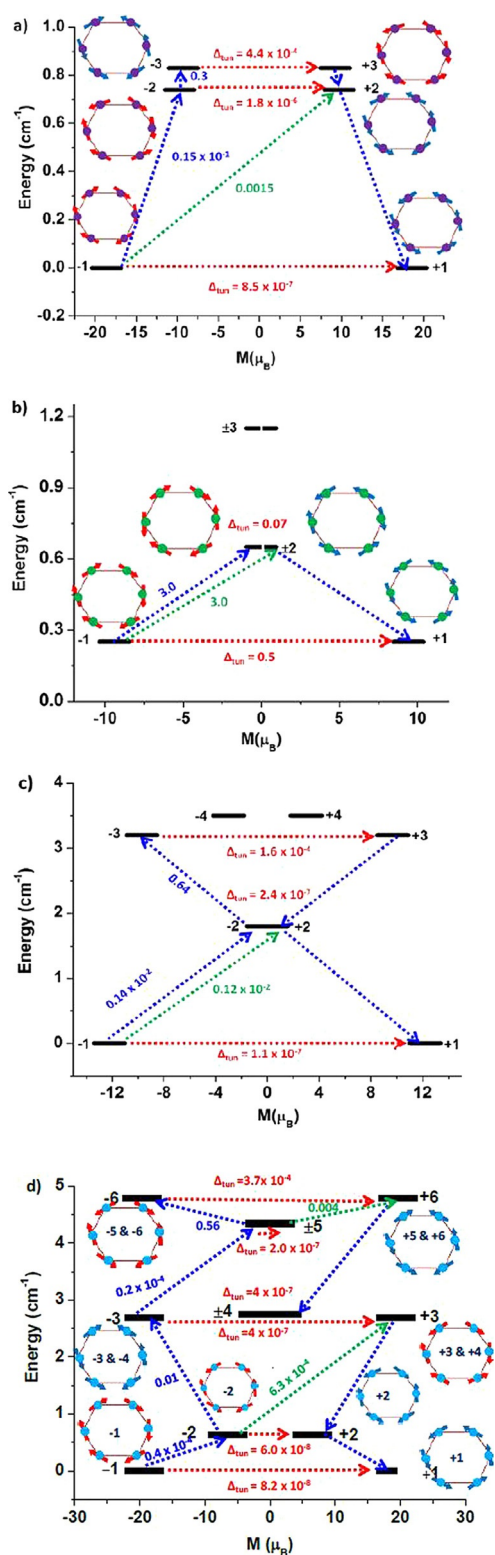


**Figure 6.** Low-lying exchange spectrum in a) **2** {Tb<sub>6</sub>}; b) **3** {Ho<sub>6</sub>}; c) **4** {Er<sub>6</sub>} and d) **5** {Dy<sub>6</sub>}. The exchange states are placed on the diagram per their magnetic moments (bold black lines). The red arrows show the tunnelling transitions (energy splitting) within each doublet state, while the green/blue arrows show the possible pathway through Orbach/Raman relaxation. The numbers at the paths are averaged transition moments in  $\mu_B$ , connecting the corresponding states. In a), b) and d) at few energy levels it provides a graphical representation of one of the corresponding non-collinear Ising quantum states, where the red/blue thick arrows at the Ln<sup>III</sup> sites indicate magnetic moment direction in toroidal form.

for 1 {Dy<sub>6</sub>}<sup>[10b]</sup> Complexes **2**, **3** and **5** are therefore classed as net toroidal moment SMTs (toroidal moment with zero conventional magnetic moment). Whereas, in **4**, the dipolar coupling is smaller than the exchange coupling, thus, not allowing the magnetic moment to be aligned in a circular form. A small tunnelling gap due to Ising nature of the anisotropy in the ground doublet in **2**, **3** and **5** also suggest that the tunnelling at the ground state is very small (see Tables S5, S6 and S8).

The orientation of the local anisotropy axes can be explained qualitatively based on the difference in electron density of the ground state  $m_j$  levels among complexes **2**–**5**. Since the electron density of the largest ground state  $m_j$  levels of Tb<sup>III</sup>, Dy<sup>III</sup> and Ho<sup>III</sup> ions are oblate in nature, to minimize the electrostatic repulsion, the  $g_{zz}$  axis of each Tb<sup>III</sup>, Dy<sup>III</sup> and Ho<sup>III</sup> ion lies along the plane of the molecule, allowing for the electron density to lie perpendicular to the direction of the axes. This arrangement results in the circular pattern and hence the toroidal magnetic moment in **2**, **3** and **5**. For **4**, the Er<sup>III</sup> ion  $m_j = \pm 15/2$  state is prolate in nature which causes the  $g_{zz}$  axis of each ion to lie perpendicular to the {Er<sub>6</sub>} wheel resulting in the absence of a circular pattern and, hence, no toroidal behaviour.<sup>[7]</sup>

The energy level at which magnetic relaxation occurs is 0.83 cm<sup>-1</sup>, 0.25 cm<sup>-1</sup> and 4.79 cm<sup>-1</sup> for **2**, **3** and **5**, respectively, indicating the toroidal magnetic moment could be blocked below this state and can be considered as the stabilization energy of the toroidal moment. We predicted earlier that the toroidal state in complex 1{Dy<sub>6</sub>}<sup>[10b]</sup> could be increased by forcing the local anisotropy axes of the Dy<sup>III</sup> ions to lie in the plane of the molecule, by modifying the ligand environment on the Dy<sup>III</sup> sites. This ligand field effect was proven by Powell and co-workers, by utilizing *rac*-1-[*N,N*-bis-(2-hydroxyethyl)amino]-2-propanol (Me-teaH<sub>3</sub>) and 2,2'-(3-aminopropylazanediy) diethanol (apadH<sub>4</sub>) ligands.<sup>[14]</sup> We also show, from the present work, we can achieve this goal by lowering the crystallographic symmetry of the crystal, in this case from trigonal to triclinic. The triclinic symmetry enforces the local anisotropy axes to be oriented at 77° to the plane of the molecular S<sub>6</sub> symmetry axis (5{Dy<sub>6</sub>}), forcing the local anisotropy axes of the Dy<sup>III</sup> ions to lie closer to the plane of the molecule, whereas it was found to be 43° in the trigonal case (1{Dy<sub>6</sub>}). Moreover, the angle ( $\theta$ ) between the orientation of magnetic anisotropy and the vector connecting two Dy centres is found to be larger for **5** (87.4°) compared to **1** (73°).<sup>[10b]</sup> This indicates that lowering the symmetry (unsymmetrical Dy...Dy bond distances) can help to improve the dipolar coupling by increasing the angle ( $\theta$ ). Lowering the crystallographic symmetry, therefore, resulted in stronger dipolar interactions between neighbouring ions (−9.2 cm<sup>-1</sup> for **5** compared to −4.2 cm<sup>-1</sup> for **1**), hence increasing the stabilization energy of the toroidal magnetic state to 4.8 cm<sup>-1</sup> (**5**) from 4.4 cm<sup>-1</sup> (**1**).

The local anisotropy axes for the non-Kramer Tb<sup>III</sup> and Ho<sup>III</sup> ions in **2** and **3** (trigonal symmetry) are found to be nearly in the plane of the molecule at  $\approx 85^\circ$  from the S<sub>6</sub> symmetry, however, the weaker dipolar coupling (see Table 4) causes some total magnetic moment (0.36  $\mu_B$  for **2** and 0.54  $\mu_B$  for **3**) in the ground state compared to the {Dy<sub>6</sub>} molecules (0.005  $\mu_B$  for **5**),



decreasing the stabilization energy of the toroidal moment by 0.83 and 0.25 cm<sup>-1</sup>, respectively. We have therefore predicted toroidal behaviour for Tb<sup>III</sup> and Ho<sup>III</sup> based {Ln<sup>III</sup><sub>6</sub>} wheels, providing rare cases of such behaviour in the non-Kramer ions.<sup>[7]</sup> The observation of toroidicity in the non-Kramer Ho<sup>III</sup> complex **3** was strongly supported by the experimental observation of S-shape in *M* versus *H* plots (see Figure 3, middle 1). Such toroidal moments in oblate Dy and Tb ions with Kramer versus non-Kramer ion nature have also been realized for heterometallic 3d–4f metallocycles by Tang and co-workers.<sup>[33]</sup>

## Conclusions and Outlook

We synthesized, structurally and magnetically characterized four {Ln<sup>III</sup><sub>6</sub>(teaH)<sub>6</sub>(NO<sub>3</sub>)<sub>6</sub>} (Ln = Tb (**2**), Ho (**3**), Er (**4**) and Dy (**5**)) wheel complexes. The *M* versus *H* plots at low fields at 2 K revealed a S-shaped curve for **3**, which suggests the presence of a toroidal moment, unfortunately this is not observed for **2** and **5**. Ab initio calculations revealed a non-magnetic ground state with a net toroidal magnetic moment for the oblate ion containing {Tb<sub>6</sub>} (**2**), {Ho<sub>6</sub>} (**3**) and {Dy<sub>6</sub>} (**5**) complexes, while in the prolate ion containing {Er<sub>6</sub>} (**4**) complex it is found to be absent. The net toroidal moment in {Tb<sub>6</sub>}, {Ho<sub>6</sub>} and {Dy<sub>6</sub>} complexes arise due to the presence of strong antiferromagnetic dipolar coupling and the high symmetry (S<sub>6</sub>) present in the molecule. The coupled states are very close in energy and in some cases strong single-ion tunnel splitting is detected causing fast relaxation of magnetization, which leads to the lack of SMM behaviour for **2–5** in zero static field. The stabilization energy of the toroidal magnetic state is found to increase in **5** {Dy<sup>III</sup><sub>6</sub>} (4.8 cm<sup>-1</sup>) compared to **1** {Dy<sup>III</sup>} (4.4 cm<sup>-1</sup>) due to an increase in dipolar coupling attributed to lowering the crystallographic symmetry (unsymmetrical Dy...Dy bond distances). Our results indicate that as well as high symmetry and dipolar coupling being key criteria for engineering toroidal moments in these six-ring species, the oblate nature of the electron density of the Ln<sup>III</sup> ion ground state play a significant role, while lowering of the crystallographic symmetry in a {Dy<sub>6</sub>} wheel leads to improved toroidal properties. To further understand the role of these criteria that decide the nature of magnetic anisotropy in clockwise/anticlockwise directions on engineering the toroidal behaviour, we are aiming to perform further experiments such as torque magnetometry, HF-EPR and NMR techniques on these complexes and these studies will be reported later.

## Acknowledgements

G.R. would like to acknowledge the financial support from SERB-DST (EMR/2014/000247) India, and IIT Bombay for the high performance computing facility. K.R.V. would like to thank the IITB-Monash Academy for research funding. K.S.M. thanks the Australian Research Council and the Australia-India Strategic Research Fund for support. Structural aspects of this research were undertaken on the MX1 beamline at the Australian Synchrotron, Clayton, Victoria, Australia.

## Conflict of interest

The authors declare no conflict of interest.

**Keywords:** dipoles · lanthanides · magnetism · symmetry · toroics

- [1] "Chapter 3: Polynuclear Lanthanide Single Molecule Magnets": J. Tang, P. Zhang in *Lanthanides and Actinides in Molecular Magnetism*, (Eds.: R. A. Layfield, M. Murugesu), Wiley-VCH, Weinheim, **2015**, pp. 61–88.
- [2] a) D. Gatteschi, R. Sessoli, *Angew. Chem. Int. Ed.* **2003**, *42*, 268–297; *Angew. Chem.* **2003**, *115*, 278–309; b) R. Sessoli, D. Gatteschi, A. Caneschi, M. A. Novak, *Nature* **1993**, *365*, 141–143; c) R. Sessoli, H. L. Tsai, A. R. Schake, S. Wang, J. B. Vincent, K. Folting, D. Gatteschi, G. Christou, D. N. Hendrickson, *J. Am. Chem. Soc.* **1993**, *115*, 1804–1816.
- [3] a) M. Evangelisti, E. K. Brechin, *Dalton Trans.* **2010**, *39*, 4672–4676; b) J. Schnack, R. Schmid, J. Richter, *Phys. Rev. B* **2007**, *76*, 054413; c) F. Torres, J. M. Hernandez, X. Bohigas, J. Tejada, *Appl. Phys. Lett.* **2000**, *77*, 3248–3250.
- [4] a) J. Tang, I. Hewitt, N. T. Madhu, G. Chastanet, W. Wernsdorfer, C. E. Anson, C. Benelli, R. Sessoli, A. K. Powell, *Angew. Chem. Int. Ed.* **2006**, *45*, 1729–1733; *Angew. Chem.* **2006**, *118*, 1761–1765; b) L. Ungur, S.-Y. Lin, J. Tang, L. F. Chibotaru, *Chem. Soc. Rev.* **2014**, *43*, 6894–6905.
- [5] a) L. F. Chibotaru, L. Ungur, A. Soncini, *Angew. Chem. Int. Ed.* **2008**, *47*, 4126–4129; *Angew. Chem.* **2008**, *120*, 4194–4197; b) S.-Y. Lin, W. Wernsdorfer, L. Ungur, A. K. Powell, Y.-N. Guo, J. Tang, L. Zhao, L. F. Chibotaru, H.-J. Zhang, *Angew. Chem. Int. Ed.* **2012**, *51*, 12767–12771; *Angew. Chem.* **2012**, *124*, 12939–12943; c) A. Soncini, L. F. Chibotaru, *Phys. Rev. B* **2008**, *77*, 220406; d) L. Ungur, W. Van den Heuvel, L. F. Chibotaru, *New J. Chem.* **2009**, *33*, 1224–1230; e) "Chapter 286: Magnetic Bistability in Lanthanide-Based Molecular Systems: The Role of Anisotropy and Exchange Interactions": D. Gatteschi, R. Sessoli, L. Sorace in *Handbook on the Physics and Chemistry of Rare Earths*, Vol. 50, (Eds.: J.-C. Bünzli, V. K. Pecharsky), Elsevier, Amsterdam **2016**, pp. 91–139; f) J. Luzon, K. Bernot, I. J. Hewitt, C. E. Anson, A. K. Powell, R. Sessoli, *Phys. Rev. Lett.* **2008**, *100*, 247205; g) M. Gysler, F. El Hallak, L. Ungur, R. Marx, M. Haki, P. Neugebauer, Y. Rechkemmer, Y. Lan, I. Sheikin, M. Orlita, C. E. Anson, A. K. Powell, R. Sessoli, L. F. Chibotaru, J. van Slageren, *Chem. Sci.* **2016**, *7*, 4347–4354.
- [6] a) A. I. Popov, D. I. Plokhov, A. K. Zvezdin, *EPL* **2009**, *87*, 67004; b) A. Soncini, L. F. Chibotaru, *Phys. Rev. B* **2010**, *81*, 132403.
- [7] K. R. Vignesh, S. K. Langley, A. Swain, B. Moubaraki, M. Damjanović, W. Wernsdorfer, G. Rajaraman, K. S. Murray, *Angew. Chem. Int. Ed.* **2018**, *57*, 779–784; *Angew. Chem.* **2018**, *130*, 787–792.
- [8] a) A. I. Popov, D. I. Plokhov, A. K. Zvezdin, *Phys. Rev. B* **2016**, *94*, 184408; b) C. Das, S. Vaidya, T. Gupta, J. M. Frost, M. Righi, E. K. Brechin, M. Afronite, G. Rajaraman, M. Shanmugam, *Chem. Eur. J.* **2015**, *21*, 15639–15650.
- [9] G. Fernandez Garcia, D. Guettas, V. Montigaud, P. Larini, R. Sessoli, F. Totti, O. Cador, G. Pilet, B. Le Guennic, *Angew. Chem. Int. Ed.* **2018**, *57*, 17089–17093.
- [10] a) S. K. Langley, B. Moubaraki, C. M. Forsyth, I. A. Gass, K. S. Murray, *Dalton Trans.* **2010**, *39*, 1705–1708; b) L. Ungur, S. K. Langley, T. N. Hooper, B. Moubaraki, E. K. Brechin, K. S. Murray, L. F. Chibotaru, *J. Am. Chem. Soc.* **2012**, *134*, 18554–18557.
- [11] I. J. Hewitt, J. Tang, N. T. Madhu, C. E. Anson, Y. Lan, J. Luzon, M. Etienne, R. Sessoli, A. K. Powell, *Angew. Chem. Int. Ed.* **2010**, *49*, 6352–6356; *Angew. Chem.* **2010**, *122*, 6496–6500.
- [12] G. Novitchi, G. Pilet, L. Ungur, V. V. Moshchalkov, W. Wernsdorfer, L. F. Chibotaru, D. Luneau, A. K. Powell, *Chem. Sci.* **2012**, *3*, 1169–1176.
- [13] K. R. Vignesh, A. Soncini, S. K. Langley, W. Wernsdorfer, K. S. Murray, G. Rajaraman, *Nat. Commun.* **2017**, *8*, 1023.
- [14] A. Baniodeh, N. Magnani, S. Brase, C. E. Anson, A. K. Powell, *Dalton Trans.* **2015**, *44*, 6343–6347.
- [15] T. M. McPhillips, S. E. McPhillips, H.-J. Chiu, A. E. Cohen, A. M. Deacon, P. J. Ellis, E. Garman, A. Gonzalez, N. K. Sauter, R. P. Hizackerley, S. M. Soltis, P. Kuhn, *J. Synchrotron Radiat.* **2002**, *9*, 401–406.
- [16] W. Kabsch, *J. Appl. Crystallogr.* **1993**, *26*, 795–800.

- [17] G. Sheldrick, *Acta Crystallogr. Sect. A* **2008**, *64*, 112–122.
- [18] G. M. Sheldrick, *SHELXL-97, Programs for X-ray Crystal Structure Refinement*, University of Göttingen, Göttingen **1997**.
- [19] L. J. Barbour, *J. Supramol. Chem.* **2001**, *1*, 189–191.
- [20] F. Aquilante, J. Autschbach, R. K. Carlson, L. F. Chibotaru, M. G. Delcey, L. D. Vico, I. F. Galván, N. Ferré, L. M. Frutos, L. Gagliardi, M. Garavelli, A. Giussani, C. E. Hoyer, G. L. Manni, H. Lischka, D. Ma, P. Å. Malmqvist, T. Müller, A. Nenov, M. Olivucci, T. B. Pedersen, D. Peng, F. Plasser, B. Pritchard, M. Reiher, I. Rivalta, I. Schapiro, J. Segarra-Martí, M. Stenrup, D. G. Truhlar, L. Ungur, A. Valentini, S. Vancoillie, V. Veryazov, V. P. Vysotskiy, O. Weingart, F. Zapata, R. Lindh, *J. Comput. Chem.* **2016**, *37*, 506–541.
- [21] B. A. Hess, C. M. Marian, U. Wahlgren, O. Gropen, *Chem. Phys. Lett.* **1996**, *251*, 365–371.
- [22] B. O. Roos, P.-A. Malmqvist, *Phys. Chem. Chem. Phys.* **2004**, *6*, 2919–2927.
- [23] B. O. Roos, R. Lindh, P.-A. Malmqvist, V. Veryazov, P.-O. Widmark, A. C. Borin, *J. Phys. Chem. A* **2008**, *112*, 11431–11435.
- [24] P. A. Malmqvist, B. O. Roos, B. Schimmelpfennig, *Chem. Phys. Lett.* **2002**, *357*, 230–240.
- [25] L. F. Chibotaru, L. Ungur, *J. Chem. Phys.* **2012**, *137*, 064112–064122.
- [26] L. Gagliardi, R. Lindh, G. Karlström, *J. Chem. Phys.* **2004**, *121*, 4494–4500.
- [27] a) A. Upadhyay, K. R. Vignesh, C. Das, S. K. Singh, G. Rajaraman, M. Shanmugam, *Inorg. Chem.* **2017**, *56*, 14260–14276; b) B. Wang, S. L. Li, D. G. Truhlar, *J. Chem. Theory Comput.* **2014**, *10*, 5640–5650.
- [28] L. F. Chibotaru, L. Ungur, *POLY\_ANISO program* **2006**, University of Leuven.
- [29] a) J. Cirera, E. Ruiz, S. Alvarez, *Chem. Eur. J.* **2006**, *12*, 3162–3167; b) M. Pinsky, D. Avnir, *Inorg. Chem.* **1998**, *37*, 5575–5582.
- [30] a) S. K. Langley, D. P. Wielechowski, V. Vieru, N. F. Chilton, B. Moubaraki, B. F. Abrahams, L. F. Chibotaru, K. S. Murray, *Angew. Chem. Int. Ed.* **2013**, *52*, 12014–12019; *Angew. Chem.* **2013**, *125*, 12236–12241; b) S. K. Langley, L. Ungur, N. F. Chilton, B. Moubaraki, L. F. Chibotaru, K. S. Murray, *Inorg. Chem.* **2014**, *53*, 4303–4315.
- [31] a) “Magnetic Ordering due to Dipolar Interaction in Low Dimensional Materials”: P. Panissod, M. Drillon in *Magnetism: Molecules to Materials IV*, (Eds.: J. S. Miller, M. Drillon), Wiley-VCH, Weinheim, **2002**, p. 235; b) J.-D. Leng, J.-L. Liu, W.-Q. Lin, S. Gomez-Coca, D. Aravena, E. Ruiz, M.-L. Tong, *Chem. Commun.* **2013**, *49*, 9341–9343.
- [32] J. J. Le Roy, L. Ungur, I. Korobkov, L. F. Chibotaru, M. Murugesu, *J. Am. Chem. Soc.* **2014**, *136*, 8003–8010.
- [33] J. Wu, X.-L. Li, M. Guo, L. Zhao, Y.-Q. Zhang, J. Tang, *Chem. Commun.* **2018**, *54*, 1065–1068.

---

Manuscript received: November 19, 2018

Revised manuscript received: January 30, 2019

Accepted manuscript online: January 31, 2019

Version of record online: February 22, 2019